Can Hα observations recover the rotational velocities of disk galaxies?

Liam Dahlberg

Division of Astrophysics

Department of Physics

LUND
UNIVERSITY

2024–EXA236

Degree project of 15 higher education credits
July 2024

Supervisors: Corentin Cadiou & Oscar Agertz

Division of Astrophysics
Department of Physics
Box 118
SE-221 00 Lund
Sweden

Abstract

The angular momentum of a galaxy is a very important concept when studying its kinematics. The two parameters that define the angular momentum are the rotational velocity of the galaxy and its dynamical mass. One of the problems with measuring the rotational velocity of a galaxy is that the galaxy may be observed at an angle. This impacts the radial velocity profile a telescope will measure. It would thus be beneficial to know if there exists an inclination correction term that, when applied to a radial velocity profile measured at an angle, gives the radial velocity profile at no inclination. If the corrections can be matched with a theoretical model of the rotational velocity of the galaxy, its dynamical mass can be estimated. Starting off with the simulated data of a galaxy from Agertz et al. (2021), which was created trying to understand the origins of galaxy structures and trends observed in the Milky Way, the rotational velocity profile at different inclinations and distances away from an observer was derived from velocities traced by $H\alpha$ emission. It was found that doing a $\cos(\theta)$ correction gives the correct shape and relatively good values when compared to the zero inclination case. The correction becomes worse the farther away the galaxy is, and also at higher inclinations. The distance was modeled using a percentage of the maximum monochromatic luminosity. This removes any effect from the cosmic redshift, noise, and interactions as the light travels toward an observer. The corrected radial velocity curves could not be matched to a theoretical model of the rotational velocity curve due to asymmetries in the radial velocity profiles. The asymmetry could be explained by the fact that Hα emitting gas can be highly turbulent, causing a significant portion of the gas to be located in regions that distort the radial velocity profile by the method used in this project. This means that the dynamical mass could not be estimated by only observing Hα emission.

Populärvetenskaplig beskrivning

Detta projekt riktar sig till att undersöka om vi kan skapa en bild av en simulerad galax, göra mätningar på den som om ett värkligt teleskop hade sett den på natthimlen, och se om dessa mätningar stämmer överens med simulerade mätvärden. Med hjälp av given data så kommer vi återskapa en bild med hög upplösning som om du själv stod framför och tittade på galaxen. Sedan kommer vi dumma ner bilden så upplösningen blir sämre och sämre tills den liknar en bild ett teleskop här på jorden hade sett. Sedan så kan vi ta reda på vad vi hade mätt av den galaxen.

Det som hjälper till att definiera galaxer är deras vinkel moment, vilket är en indikator på hur starkt de roterar. Anledningen till varför vinkel moment är bra är för att det beror på massan, storleken och rotations hastigheten av galaxen. Dessa tre komponenter tillsammans är unikt för alla galaxer. När en galax har blivit simulerad så vet vi garanterat vilket vinkel moment den har, alltså har vi redan mycket information som definierar galaxen som vi kan arbeta med. Däremot när teleskop samlar mätdata så observerar teleskop inte allt ljus, utan det är begränsat. Vi väljer alltså att titta på hur starkt ljuset från vissa våglängder är i ett spektrum, mer specifikt Hα som har en våglängd på ca 656nm. Detta uppkommer när en elektron övergår från den tredje energi-nivån till den andra i väte. Anledningen till att vi väljer just Hα är för att den är väldigt förekommande i alla galaxer. Vi samlar alltså bara in ljus och information som kommer från Hα.

Så med hjälp av vinkel momentet och ljus-styrkan från Hα så kan vi ta fram information om galaxen som ett teleskop hade mätt. De mest intressanta för oss är galaxens massa och vad vi kallar för galaxens "radial hastighets profil". Radial hastighet är hastigheten antingen direkt ifrån oss eller direkt emot oss. Alla punkter i en galaxas rör sig med en hastighet ifrån oss eller emot oss beroende på hur långt ifrån mitten av galaxen de är. Vad en "radial hastighets profil" då innebär är en graf där vi ser radial hastigheten som en funktion av avståndet från mitten av galaxen. Problemet är tyvärr att i verkligheten galaxer kan vara vinklade, vilket betyder att vi inte kan få en sann radialhastighets profil. Vi kan då se om vi kan ta fram en faktor som är beroende av vinkeln så att om vi vet hur mycket galaxen är vinklad så kan vi ta fram "radial hastighets profilen" som om galaxen inte var vinklad.

Contents

1 Introduction **2**

2 Theory **4**
- 2.1 The emission of Hα-photons . . . 4
- 2.2 Galaxy evolution . . . 5
- 2.3 The VINTERGATAN simulation . . . 5
- 2.4 YT . . . 6
- 2.5 Telescope observations . . . 6

3 Method **8**
- 3.1 Acquiring Data . . . 8
- 3.2 Luminosity-Weighted Average Velocity Maps . . . 9
- 3.3 Reorienting The Data . . . 10
- 3.4 Radial Velocity Profiles . . . 11
- 3.5 Rotational Velocity Profiles . . . 12

4 Results **14**
- 4.1 Validating the alternative method . . . 14
- 4.2 Spatial Manipulation . . . 15
- 4.3 Observational measurements . . . 17
- 4.4 Inclination Corrections . . . 18
- 4.5 Theoretical outcome . . . 18

5 Discussion **23**

Chapter 1

Introduction

The evolution of galaxies has been studied since the days of early 20th-century astronomers, such as Edwin Hubble (Hubble 1936), Fritz Zwicky (Zwicky 1933) and George Gamow (Alpher et al. 1948), (e.g Press & Schechter 1974; Binney & Tremaine 1987; Brinchmann et al. 2004). Through a better understanding of the evolution of galaxies, we gain a better understanding of how The Milky Way came to form into what we see today. We also gain a better understanding of the inner workings of other galaxies which will further the research of our universe. The way this research is conducted is by creating simulations based on predictions of initial conditions together with internal processes and external events and seeing whether the simulations match modern observations of galaxies (Abadi et al. 2003; Governato et al. 2007). The initial conditions can include properties such as density, metallicity, temperature, and more depending on what type of simulation one decides to perform. Internal processes can include star formation rate (Schmidt 1959; Tinsley 1980), and supernovae explosions (Perlmutter et al. 1999). An example of an external event that can be included in the simulation is another galaxy colliding with the simulated galaxy in focus (galaxy merger) (Naidu et al. 2021). If a galaxy has successfully been recreated through a simulation, it means that data can be gathered from the simulated galaxy instead of the physical galaxy to gain a deeper understanding of properties that would otherwise be inaccessible, depending on what information the telescope observing the galaxy is designed to gather. However, to get accurate data, it is necessary to ensure that the simulated galaxy correctly represents the galaxy it attempts to replicate.

The normal procedure for testing a theory in science is that you make a prediction based on an already existing theory or an existing model, and then perform an experiment in a lab and see if the outcome matches the prediction. Astrophysicists need one additional tool, simulations. They come up with a theory and create a simulation based on said theory. They can then gather data from a telescope, analyze that data, and compare it to the simulated model. With the necessary initial conditions and applied physical concepts, one can simulate the past conditions under which astrophysical objects came into existence, what made them evolve into what they are today, and how they will behave in the distant future. They can study a star's internal processes, a meteor's trajectory, and the

kinematics of complex planetary systems. Moreover, observations with telescopes allow astrophysicists to collect data that describe how the systems looked and behaved when the light was emitted. However, light that has already been emitted cannot be observed again. Thus, astrophysics requires the use of simulations because we cannot definitively know how things looked before modern observations. On the timescale that humans have existed and been able to document their findings, we have only experienced a mere fraction of the time it takes for astrophysical objects to evolve. This means we cannot know for certain how space looked before we existed. However, through modern observations and simulations, theories about the past can gain increased validity.

One of the many emission lines one may choose to investigate when observing a galaxy is the $[H\alpha]\lambda6564.6$ Å emission line, which the telescope KMOS (K-band Multi Object Spectrograph) is partially designed to observe. Since KMOS operates in the 8'000-25'000 Å range, Hα needs to be redshifted enough to fall within this range (Sharples et al. 2003). In this thesis, it is assumed the redshift of the simulated galaxy is high enough for KMOS to observe Hα emission. Hα was chosen due to its high abundance (Ashraf et al. 2023) which makes it good to study as a tracer. Because of the high abundance, it is easier to identify Hα lines in any measured spectra than many other emission lines. For this reason, Hα is often selected for spectroscopic surveys (e.g Geach et al. 2008; Swinbank et al. 2017; Ashraf et al. 2023).

From measured spectra where Hα has been identified, one can use Doppler Shift on the Hα measurements to determine the radial velocity along the major rotational axis of the galaxy (Swinbank et al. 2017). If the receding velocity of the galaxy is known, it can be subtracted from the observed radial velocity so that the center of the galaxy is the rest frame to plot a radial velocity profile (RVP). Since galaxies can be observed at different inclinations, if the inclination is known then the RVP can be corrected to represent a zero-degree inclination RVP. From this, a rotational velocity curve (RVC) can be derived. From the RVC of a galaxy, parameters such as the radius, dynamical mass, and velocity dispersion of the galaxy can be measured. These parameters can then be compared with real-life observations in order to see if they are a match. This thesis will attempt to determine what measurements a real telescope would gather from solely Hα emission in a simulated galaxy. This will be done by examining what Hα emission can tell us about the kinematics of gas in the galaxy by assuming a futuristic telescope with better specs than any telescope today, and how these measurements can be used to determine the RVP at different inclinations, which will then be inclination corrected. All the inclination-corrected RVPs will be compared to two independent theoretical RVCs. If the RVC of the galaxy based on Newtonian mechanics can be recovered from the measured RVPs, properties such as the mass dynamical of the galaxy can be derived.

Chapter 2

Theory

2.1 The emission of Hα-photons

The primary cause of $H\alpha$ emission is through collisional excitation (Ejdetjärn et al. 2022). This means a hydrogen electron with principal quantum number n=1 or 2, gains energy from a particle colliding with it. This transfers energy to the electron, exciting it. The extra energy may be enough to make the principal quantum number of the electron go to n=3. The electron can then de-excite down to n=2 which emits an $H\alpha$ photon, meaning a photon of wavelength 6564.6 Å.

For the frequency of this process to occur to the point that it becomes highly abundant, the temperature needs to be very large, around 10^4 K (Ejdetjärn et al. 2022). At this temperature, the rms velocity of electrons is large enough to make collisions happen frequently. This means that $H\alpha$ is a good tracer for hot regions of space. One key thing to note, however, is that Hα can be observed in cold regions, where it is not a good tracer. Hα emitting gas can outflow towards cold regions due to supernova explosions or pressure gradients caused by temperature differences. Thus observing $H\alpha$-emission from cold regions does not necessarily reflect the kinematics of the galaxy. This makes an analysis of a galaxy become more difficult the more face-on (larger inclination) it appears since more cold regions will be visible.

If a galaxy is observed edge-on, the photons emitted from gas in any cold region are mixed in with the photons emitted from the hot regions, meaning they do not become a problem when creating an edge-on RVP. Since reality isn't easy, galaxies may appear inclined when observed by a telescope, meaning we cannot measure an edge-on RVP from them. One can try to correct an RVP for the inclination, seeing if an edge-on RVP can be recovered. The problem with this is that a given galaxy will not appear at different inclinations, only one. This means that only one RVP can be measured, which cannot be compared to an edge-on RVP if the galaxy is inclined. However, in a simulated environment, the inclination can be chosen and altered. An RVP can thus be measured at different inclinations, and can

therefore be compared to each other after having been inclination corrected. The better the match with the edge-on RVP, the less effect gas from cold regions has on the RVP.

2.2 Galaxy evolution

Although galaxies come in a variety of shapes and sizes, some patterns common to many galaxies have emerged. It was these patterns that led Edwin Hubble in 1936 to put forth the idea of the Hubble Sequence (Hubble 1936). Galaxies were grouped into ellipticals, normal spirals, barred spirals, and irregulars. Normal spirals and barred spirals can be grouped as disk galaxies. What makes these disk galaxies form from diffuse gas is due to the existence of a dark matter halo (Schneider 2006). The gas within the dark matter halo contains angular momentum, and as it gets gravitationally pulled together towards the center, the total angular momentum must be conserved. This process also requires that the gas cools and loses pressure support, ensuring the stability of the system, assuming no dust or gas gets added or removed. This naturally leads to the gas forming a rotating disk with an angular momentum vector pointing perpendicular to the surface of the rotating disk (Mo et al. 1998). What determines the resulting rotational velocity will be the dynamical mass of the galaxy, meaning the mass of individual particles together with the mass of the dark matter halo. Although a rotating disk will of course have rotational velocity, we cannot measure the total velocity of each particle through light emission. What we can measure via light emission, is the radial component of the velocity as seen by an observer due to the Doppler Effect.

2.3 The VINTERGATAN simulation

The data used in this thesis was generated by Agertz et al. (2021) in their simulation VINTERGATAN. In this simulation, they studied the origins of chemical trends and structure of a galaxy with the same mass as the Milky Way based on modern-day observations of our galaxy. The simulation was a cosmological hydrodynamic+N-body zoom-in simulation, created using a supercomputer. The set of initial conditions was generated using the MUSIC code (Hahn & Abel 2011) with cosmological constants $H_0 = 70.2$ km s^{-1} Mpc^{-1}, $\Omega_m = 0.272$, $\Omega_\Lambda = 0.728$, and $\Omega_b = 0.045$ assuming a flat Λ-cold dark matter cosmology. Most importantly the total mass in the simulation is that of the Milky Way. This mass was spread out over a periodic box of size 85Mpc. The simulation then evolved through time to see if the emerging galaxy would display similar properties as the Milky Way. The star formation rate density $\dot{\rho}_*$ of a cell was calculated by

$$\dot{\rho}_* = \epsilon_{ff} \frac{\rho_g}{t_{ff}} , \tag{2.1}$$

where ρ_g is the gas density, $t_{ff} = \sqrt{3\pi/32G\rho_g}$ is the local free-fall time, and ϵ_{ff} is the local star formation efficiency per free-fall time of the gas in the cell. Though Eq. 2.1 was only

used given that $\rho > \rho_{SF}$ ($\rho_{SF} = 100\text{cm}^{-3}$ is the star formation threshold) and $T_{gas} < T_{SF}$ ($T_{SF} = 100$ K being the maximum allowed temperature of star-forming gas) inside a cell.

The data from the VINTERGATAN simulation is volumetric, meaning that every cell in the simulation has 3D spatial coordinates. Each cell in turn contains information such as the mass of gas, stars, and dark matter. They also contain particle number density, temperature, x, y, and z velocity components, metallicity, and more. The data from the galaxy produced in the VINTERGATAN simulation will be assumed to be the absolute truth, meaning no uncertainties.

2.4 YT

The present study utilized data produced by the VINTERGATAN simulation, loading it into Python with the help of the Python library YT created by Turk et al. (2011). It is a library that allows one to easily handle large volumetric data sets in many unique ways. YT can be used to cut down data sets into relevant sections, for example a single galaxy from a cosmological simulation. When a data set has been created using YT, all necessary parameters can then be extracted into numpy-arrays. This is so that we can determine what we would measure from an emission line since YT does not have any function to do so. Simulating emission lines and the troubles that come with it has been a topic of discussion for a long time (Olsen et al. 2018). For this reason, the Hα-emission for this project will be determined using a simplified approach.

2.5 Telescope observations

As a telescope gathers light, it can measure the wavelength and the intensity of the light. This then creates a spectrum that spans over a range of wavelengths dependent on the telescope. The broader the interval the less information it can gather about specific peaks, but more wavelengths can be investigated. And on the other side, the narrower the interval the less information it can gather about other wavelengths, but more precise measurements of the peaks that do appear. Any wavelength outside the range of a telescope will consequently not be detected. But due to the cosmic redshift z, wavelengths emitted from faraway galaxies will get elongated. Some wavelengths that otherwise would not be able to be detected due to a too small rest-wavelength, can become detectable. The opposite case also applies, a wavelength that would fall within the range of what a telescope can detect gets shifted to the point that it can no longer be detected.

Looking at one particular peak wavelength, $\lambda_{observed}$: here, the data points will be spread out partially due to the Doppler effect, which is called Doppler Broadening. This is caused by the movement of the emitter relative to an observer. One can thus take data from a

spectrum and calculate their respective velocities using the cosmic redshift

$$z = \frac{\lambda_{observed} - \lambda_{rest}}{\lambda_{rest}} \approx \frac{v}{c} \, . \tag{2.2}$$

Since λ_{rest} is determined by the peak that is chosen to be investigated and $\lambda_{observed}$ is measured, everything is known in order to solve for the corresponding velocity and redshift. The approximation in the latter part of Eq. 2.2 is only valid if z is very small, which is the case for many galaxies. Though the velocities cannot be measured as a continuous quantity for the observed wavelengths, but instead are discretized to Δv. This is determined by the spectral resolution R of the telescope via

$$\Delta v = \frac{c}{R} \, , \tag{2.3}$$

where c is the speed of light.

As telescopes observes a region of space, they can only take in so much information. The more resolved an object is, the more detailed information can be gathered. What determines if an image is resolved or not mainly lies in how many pixels it covers. The three things that determine how many pixels an object covers are (1) the size of the object, (2) the distance to the object, and (3) the image resolution of the telescope. All these points mean that observing a large object that is close (for example a planet in our solar system) will be more resolved than an image of a smaller object farther away (for example an asteroid outside our solar system).

A telescope equipped with a spectrometer will measure a unique spectrum for each pixel. However, such detectors will not resolve all brightness levels in order to reduce the influence of noise. For this reason, telescopes have a certain sensitivity for every wavelength. If the intensity of light that reaches the telescope is too weak, it is not registered, and the information will be lost to the universe. The intensity of light will be dependent on processes inside the observed object (such as the nuclear fusion in a star) and light coming from behind that may pass through (such as light from supernovae passing through a nebula), but also the distance to the observed object since the intensity decays over distance by the inverse square law.

Chapter 3

Method

3.1 Acquiring Data

The data used in this project was created in the VINTERGATAN simulation by Agertz et al. (2021). The data was accessed by loading the generated data file into Python using YT (Turk et al. 2011). YT is a library that can perform operations on volumetric data in a relatively quick manner which makes it optimal to use for this project. However, one needs to define their own function, using YT, that can calculate the $H\alpha$-luminosity of a cell. The luminosity of $H\alpha$, $L_{H\alpha}$, can be calculated by

$$L_{H\alpha} = \epsilon_{H\alpha} \times V \ , \tag{3.1}$$

where $\epsilon_{H\alpha}$ is the $H\alpha$ emissivity and V is the volume of a cell. In turn, $\epsilon_{H\alpha}$ can be calculated by

$$\epsilon_{H\alpha} = n_e n_H h\nu_{H\alpha} q \ , \tag{3.2}$$

(Ejdetjärn et al. 2022) where n_e is the electron density, n_H is the neutral hydrogen density, $h\nu_{H\alpha}$ is the energy of a $H\alpha$ photon and q is the emission rate defined by

$$q = q_{coll}\left(T\right) + q_{recomb}\left(T\right) \ . \tag{3.3}$$

In Eq. 3.3, the collisional excitation rate q_{coll} is calculated by

$$q_{coll}\left(T\right) = \frac{1.2 \times 10^{-6}}{T^{0.5}} \left(\frac{T}{11.2}\right)^{0.305} \times exp\left(\frac{-h\nu_{H\alpha}}{kT}\right) \ , \tag{3.4}$$

and the recombination rate q_{recomb} is calculated by

$$q_{recomb}\left(T\right) = \epsilon^{B}_{H\alpha}\left(T\right) \alpha_B\left(T\right) \ , \tag{3.5}$$

where

$$\epsilon^{B}_{H\alpha}\left(T\right) = 8.276 \times 10^{-8} - 7.46 \times 10^{-3} \log_{10}\left(T \times 10^{-4}\right) + 0.45101 \left(T \times 10^{-4}\right)^{-0.1013} \ , \tag{3.6}$$

is the emitted rate of Hα, and

$$\alpha_B(T) = 2.753 \times 10^{-14} \left(\frac{315614}{T}\right)^{1.5} \left(1 + \left(\frac{315614}{T}\right)^{0.407}\right)^{-2.42}, \tag{3.7}$$

is the probability that the cascade from hydrogen recombination, called case B recombinations, emits an Hα photon. When Eq. 3.2 was defined as a YT function, it was used to calculate the $H\alpha$-luminosity of each cell provided n_e, n_H, T, and V are known in each cell, which it is in the provided datafile.

Other than the parameters used to calculate $L_{H\alpha}$ as mentioned above, the data used in this project included

- the x-, y-, z-position,
- the x-, y-, z-velocity,
- and the total mass

of each cell.

3.2 Luminosity-Weighted Average Velocity Maps

Another function YT has is it can create projection plots. With Eq. 3.2 defined, it could generate a luminosity-weighted average velocity map. An alternate method, not using any YT function, was created to try and match the velocity map YT produced in order to validate the alternative method. This is so the data could be worked with outside of YT, being able to operate on it using *Numpy* and *Matplotlib* and other Python libraries and functions. The four quantities used to create a luminosity-weighted velocity map, both using YT and the alternate method, are

1. The x-position, x,
2. the y-position, y,
3. the radial velocity, v_z,
4. the monochromatic luminosity, L_ν.

YT generated a projection plot by using its projection plot function already defined in the library. The inputs are the center of the dataset, the desired radius, the quantity to plot (v_z), and the weight ($L_{H\alpha}$). The alternate method instead used these quantities to generate a weighted 3D-histogram with $L_{H\alpha}$ as a weight and x, y, v_z as the bins. The number of x and y bins will determine the image resolution, meaning for example that 100 x-bins and 100 y-bins create a 100x100 pixel image. The bin size of v_z, Δv_z, reflects the spectral resolution R of a telescope by the relation given in Eq. 2.3. Once the 3D-histogram had

been generated using this information, the luminosity-weighted average velocity of each pixel was calculated, which is the weighted average of a 1D-histogram in v_z for a fixed x and y bin. The weighted average was calculated by

$$v_{av} = \frac{\sum_i L_{\nu,i} v_i}{\sum_i L_{\nu,i}} \, , \tag{3.8}$$

where v_i is the bin center of bin i with total monochromatic luminosity $L_{\nu,i}$ as the bin hight. This was used to plot a heatmap with the x and y bins as the $x-$ and $y-$axis in the plot respectively, and the luminosity-weighted average radial velocity is the heat axis.

3.3 Reorienting The Data

The data needed to be oriented in such a way that an RVP could be measured from the luminosity-weighted average radial velocity map using the alternate method previously described. The data first needed to be centered. The center of the final data set was to be the position of the center of mass of the galaxy, which is calculated by

$$\vec{r}_{com} = \frac{\sum_i m_i \vec{r}_i}{\sum_i m_i} \, , \tag{3.9}$$

where m_i is the total mass of the individual cells and $\vec{r}_i$ is the cells position vector. The data set was taken from a spherical data set with a pre-determined center. This pre-determined center may not have been the actual center of mass of the galaxy: thus, the actual center of mass was calculated using the first iteration of the data set. A second iteration of the data set was generated using the previously calculated center of mass as the new center of the data set. This process was repeated a number of times to get a more accurate center of mass as the center of the data set. The center of mass position was then subtracted from the whole data set to spatially center the data with respect to the center of the galaxy. The center of mass velocity for the data set was was then calculated in a similar way to Eq. 3.9 using the cell velocity $\vec{v}_i$ instead of the position $\vec{r}_i$

$$\vec{v}_{com} = \frac{\sum_i m_i \vec{v}_i}{\sum_i m_i} \, , \tag{3.10}$$

and was then subtracted from the final data set. To get an RVP, the galaxy needs to be viewed edge-on, and so the data was rotated in such a way to make this the case. The angular momentum vector, $\vec{J}$, of a galaxy will be pointing perpendicular to the plane of rotation (Mo et al. 1998). The angular momentum can be calculated by

$$\vec{J} = \sum_i \vec{r}_i \times (m\vec{v}_i) \, . \tag{3.11}$$

This was used to define a new coordinate system, which we call the primed system. In this primed system, the normalized $\hat{z}'$ unit vector is defined by

$$\hat{z}' = \frac{\vec{J}}{\left|\vec{J}\right|} \, . \tag{3.12}$$

After this, an arbitrary vector not parallel to $\hat{z}'$ was defined and used to take the cross-product with $\hat{z}'$ to get the direction of x'. Normalizing this new vector creates $\hat{x}'$. Taking the cross product between $\hat{z}'$ and $\hat{x}'$ will give $\hat{y}'$. These new unit vectors were used to create a transformation matrix, T

$$T = \begin{pmatrix} \hat{x}'_x & \hat{y}'_x & \hat{z}'_x \\ \hat{x}'_y & \hat{y}'_y & \hat{z}'_y \\ \hat{x}'_z & \hat{y}'_z & \hat{z}'_z \end{pmatrix} . \tag{3.13}$$

Since every cell has a position vector $\vec{r}$, the data set was transformed into the primed coordinate system by multiplying every cells position vector with T

$$\vec{r}' = T\vec{r} \tag{3.14}$$

3.4 Radial Velocity Profiles

Real telescopes have a sensitivity for the light they can observe. This can be represented in a simulation in different ways. The way it was done in this project was to determine the maximum monochromatic luminosity in the whole velocity map, and set the minimum detectable monochromatic luminosity as a percentage, p, of this

$$L_{\nu,min} = pL_{\nu,max} . \tag{3.15}$$

This will remove pixels that are too dim to be noticed by a telescope. In theory only the gas of the galaxy is luminous enough to be detected.

After having limited the data, an RVP was created by plotting the velocities along the $z' = 0$ axis of the velocity map as a function of the distance from the center of mass, meaning it shares the same x-axis as the RVP. This is the *true* RVP in the sense that we observe the galaxy perfectly edge-on. The galaxy was then rotated to different inclinations, θ, about the z'-axis in an analogous way to Eq. 3.14

$$\vec{r}_\theta = R\vec{r}' \tag{3.16}$$

where the rotation matrix R for an inclination θ is defined by

$$R = \begin{pmatrix} 1 & 0 & 0 \\ 0 & \cos(\theta) & -\sin(\theta) \\ 0 & \sin(\theta) & \cos(\theta) \end{pmatrix} . \tag{3.17}$$

Once the galaxy had been rotated at different inclinations, an RVP was again created for each one using the alternative method. Since the data had been rotated, the average velocities along the line of sight will have decreased. These new RVPs were then inclination corrected into the *true* RVP by

$$v_{x'} = \frac{v_\theta}{\cos(\theta)} , \tag{3.18}$$

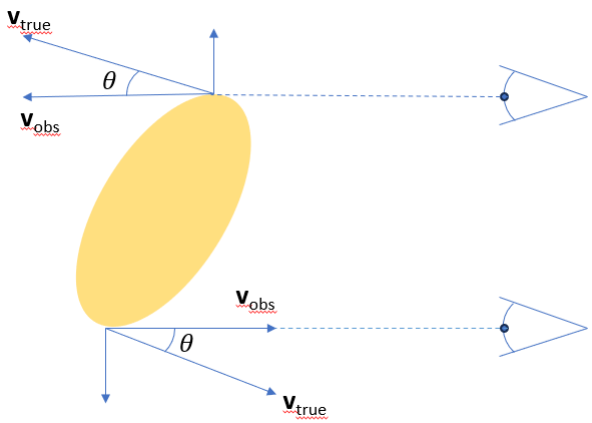

Figure 3.1: A galaxy (yellow oval) observed at an angle θ by two observers (two eyes to the right). The motion of the galaxy has been subtracted and so the observed velocity is the rotational velocity of the galaxy. The true velocity v_{true} has been split up into two right-angled components where the observed velocity v_{obs} has been marked.

where $v_{x'}$ is the true radial velocity and v_θ is the radial velocity at an inclination. An illustration of why this should work in theory is presented in Fig. 3.1.

A reason an inclination corrected RVP might differ from the *true* RVP is due to the cold regions being more prevalent. As mentioned before, Hα gas from these regions do not reflect the kinematics of these cold regions

3.5 Rotational Velocity Profiles

The *true* RVP is similar to the RVC of a galaxy, but from different observational points of view. Viewing a galaxy edge-on means one observes the radial velocity, and observing face-on means one observes the rotational velocity. There are two methods that were used in this project to determine the RVC of the galaxy. The first method was to use the known position and velocity vectors of each cell to determine the rotational velocity, v_ϕ, of each cell

$$v_\phi = -v_x \sin(\phi) + v_y \cos(\phi) \tag{3.19}$$

where the angle ϕ is defined by

$$\phi = arctan2(y, x) \ . \tag{3.20}$$

Once v_ϕ had been determined for all cells, the average along different radii was determined and used to plot an RVC.

Assuming a completely circular orbit, Newtonian mechanics was used to determine the circular velocity as a function of the radius

$$v_c = \sqrt{\frac{GM(< R)}{R}} \, . \tag{3.21}$$

where $M(< R)$ is the total mass within a radius R of the galaxy, and G is Newton's gravitational constant. Both methods plot the rotational velocity as a function of the radius. If the orbit is indeed circular, then the two RVCs should align. In order to turn them into a function of the distance from the center, like in the RVPs, they were first duplicated and had both axes negated and then plotted together with the originals. These new RVPs were then compared to the different inclination-corrected RVPs previously derived.

Chapter 4

Results

4.1 Validating the alternative method

The data file was obtained from the VINTERGATAN simulation (Agertz et al. 2021). A position of $(x, y, z)_{center} = (35603.322015, 37764.883864, 38473.463424)$kpc was chosen as an initial estimate of the center of the galaxy. This was used as the center for the data set together with a radius of 15 kpc to produce a spherical data set using YT. From this dataset, the velocity projection in Fig. 4.1 was produced using the $z - direction$ as the radial direction.

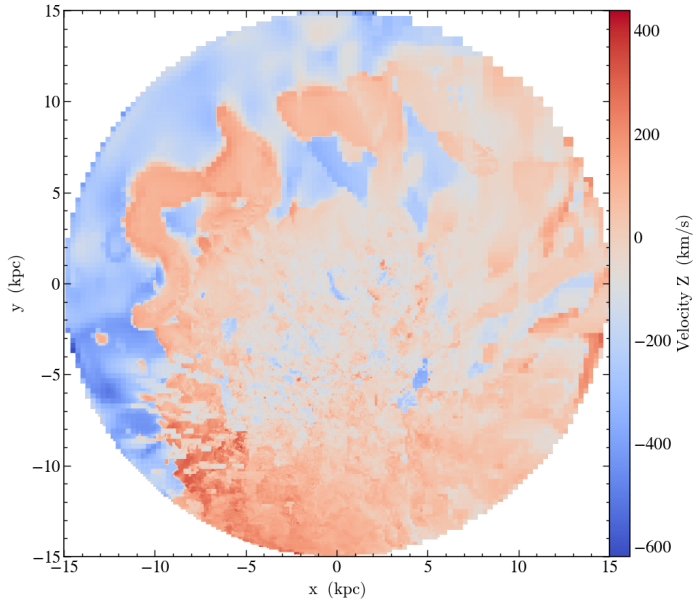

Figure 4.1: The $H\alpha$ luminosity weighted v_z velocity. This plot was created using YT by taking the data straight from the source file. The data was automatically spatially centered in the plot.

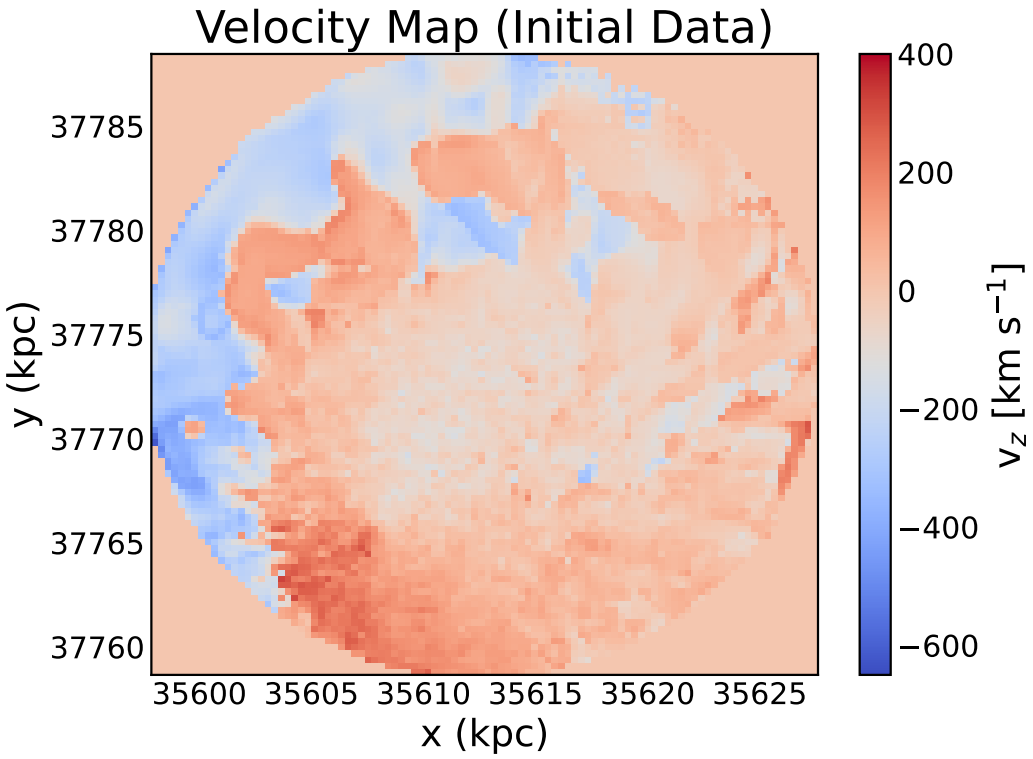

Figure 4.2: Recreated velocity map displaying a structure similar to that produced by YT. This plot has taken the position coordinates from the simulation and has not yet been spatially centered as it has in the YT image.

Fig. 4.2 shows a similar image that was produced using the alternate method outlined in the method section. An image resolution of 100x100 pixels was chosen so that the image was not too blurry to get any significant data from it. A spectral resolution of $R = 150'000$ was chosen for the same reason and corresponds to a velocity resolution of $\Delta v = 2$km/s using Eq. 2.3. These do not represent the specs of any telescope today, but might be attainable in the future.

4.2 Spatial Manipulation

We call the data set that was used to produce Fig. 4.2 "the first iteration". Using this data set, the center of mass was calculated a total of 13 times using Eq. 3.9, each new iteration using the previous iteration's center of mass as the data center. The radius was kept at 15kpc through each iteration. Table 4.1 presents the progression of the center of mass for each iteration.

Data Iteration	$\vec{r}_{COM}[kpc]$
1	(35609.683548, 37768.338827, 38473.519468)
2	(35608.336624, 37766.422908, 38474.751620)
3	(35607.976012, 37765.941125, 38475.030486)
⋮	⋮
11	(35607.853693, 37765.779696, 38475.111478)
12	(35607.853692, 37765.779696, 38475.111479)
13	(35607.853692, 37765.779696, 38475.111479)

Table 4.1: The position of the center of mass through different iterations of the dataset. A converging value within a thousand of a parsec becomes apparent after the 13th iteration. This determines an accuracy of up to 6 decimal places for the other measurements in this project.

Once the position of the center of mass had converged to $\vec{r}_{COM} = (35607.853692, 37765.779696, 38475.111479)$kpc, the velocity of the center of mass was calculated from the 13th iteration of the data set to $\vec{v}_{COM} = (-99.122633, 34.547427, 115.127650)$ km/s using Eq. 3.10. Both of these values for the center off mass were then subtracted from the 13th iteration of the dataset. Fig. 4.3 shows the newly centered data set.

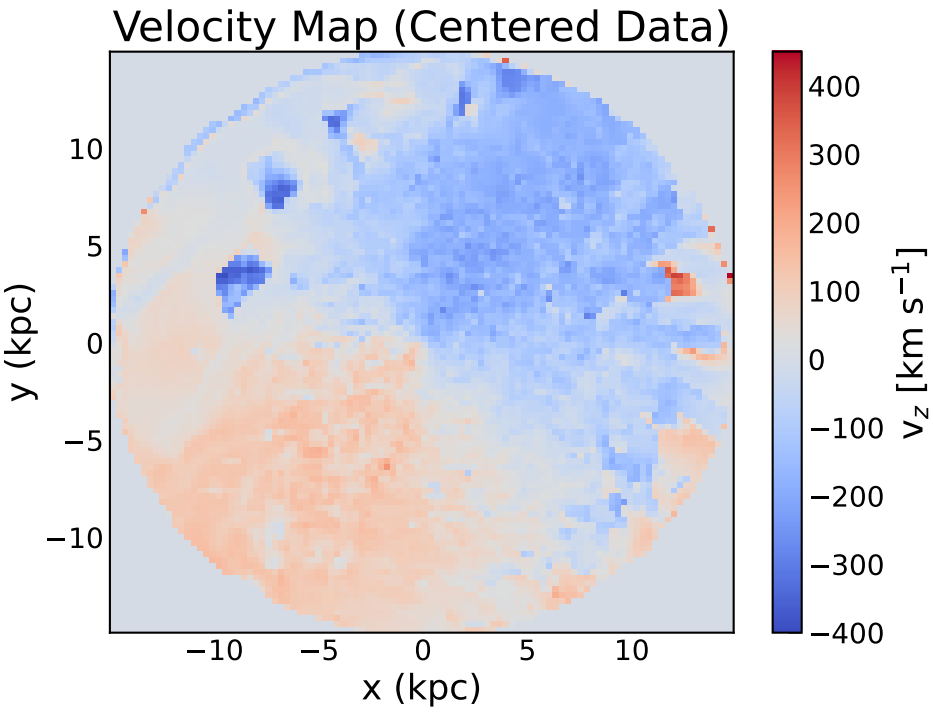

Figure 4.3: The center of the galaxy has been found and allocated to the center of the coordinate system. The velocity has also been shifted to be relative to the center of mass. The radius of the data set was set to 15kpc.

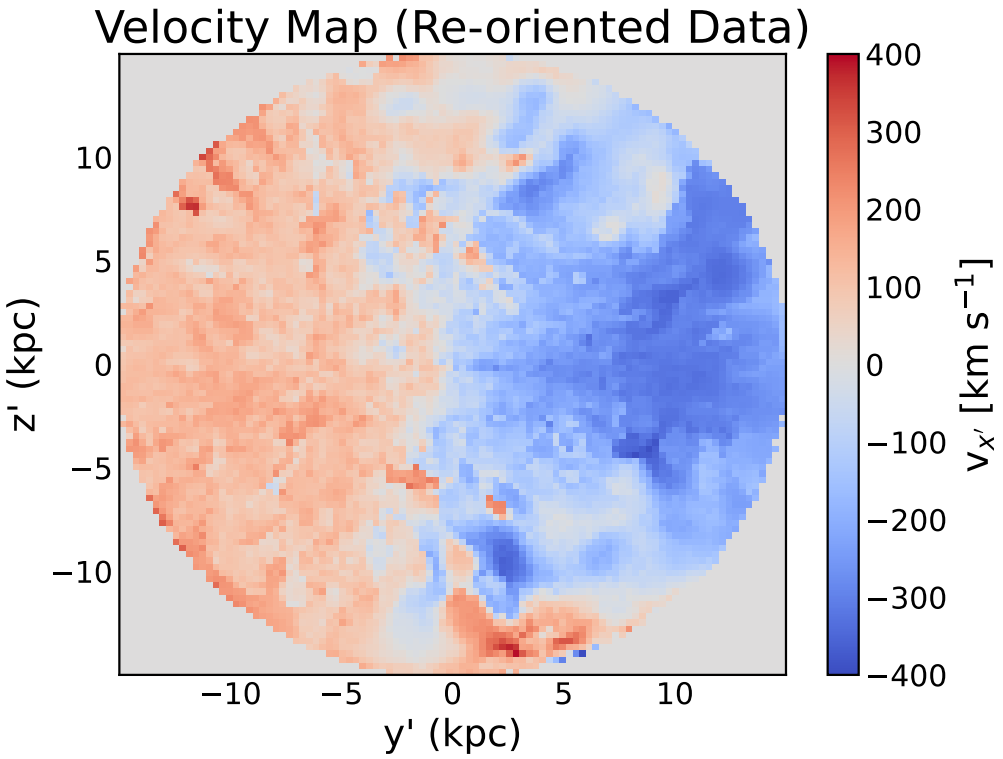

Figure 4.4: Velocity projection plot with x' as the radial direction. One can see clearly the two halves of the galaxy split at the center. One half rotating away from us (left half) and one half rotating towards us (right half).

When the data was centered both in terms of position and velocity with respect to the center of mass of the galaxy, the angular momentum vector was calculated. Using Eq. 3.11, $\vec{J} = (-6.187012, 4.428339, -6.471417) \cdot 10^9$ kpc kg km s^{-1}. Using this as the new z-direction, $\hat{z}'$, the data was rotated. Fig. 4.4 shows the resulting final spatial configuration.

4.3 Observational measurements

The maximum monochromatic luminosity, $L_{\nu,max}$, was determined from the data set in Fig. 4.4. This was done by finding the largest bin height out of all the histograms. Fig. 4.5 shows the histogram which contains the largest bin height. The bin height value is $L_{\nu,max} = 9.87 \cdot 10^{41}$ erg s^{-1} Hz^{-1}. A minimum detectable limit of 1% (p=0.01) and 0.1% (p=0.001) respectively of this was set using Eq. 3.15. This meant $L_{\nu,min,1\%} = 9.87 \cdot 10^{39}$ erg s^{-1} Hz^{-1} and $L_{\nu,min,0.1\%} = 9.87 \cdot 10^{38}$ erg s^{-1} Hz^{-1}.

Adopting these luminosity limitations, the projection plots were reduced to what is seen in Fig. 4.6. The projection plots are presented with their corresponding RVP to the right

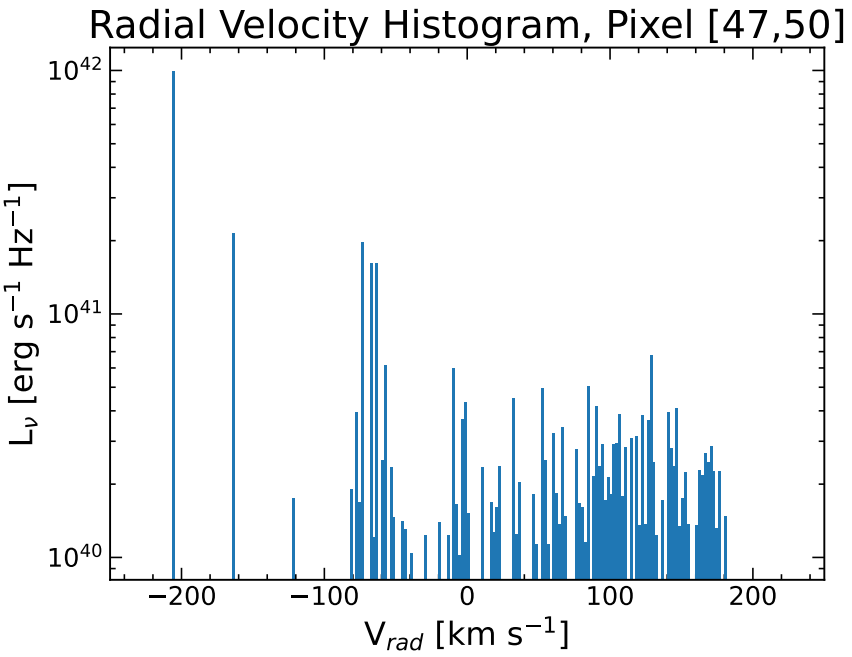

Figure 4.5: The histogram from which L_{max} was taken from. The pixel coordinates are (x,y) = (47, 50). The binsize for the velocity-axis is $\Delta v = 2$km/s. The weighted average velocity in this histogram is $v = -35.39$km/s

of them.

4.4 Inclination Corrections

As shown in Fig. 4.7, both limited data sets were then rotated at $15°, 30°, 45°, 60°$ and $75°$ inclinations. The RVP was plotted at each inclination. Each RVP was then inclination-corrected using Eq. 3.18. Fig. 4.8 shows the results.

4.5 Theoretical outcome

The data set which was not luminosity-limited reduced was then used to produce two sets of theoretical RVCs. One RVC was produced using Newtonian mechanics (focusing on the mass and position of the cells) and one was using vector analysis (focusing on the velocity and position vectors of the cells). Eq. 3.19 and Eq. 3.21 were used independently of each other to produce two RVCs, both of which are presented atop each other in Fig. 4.9.

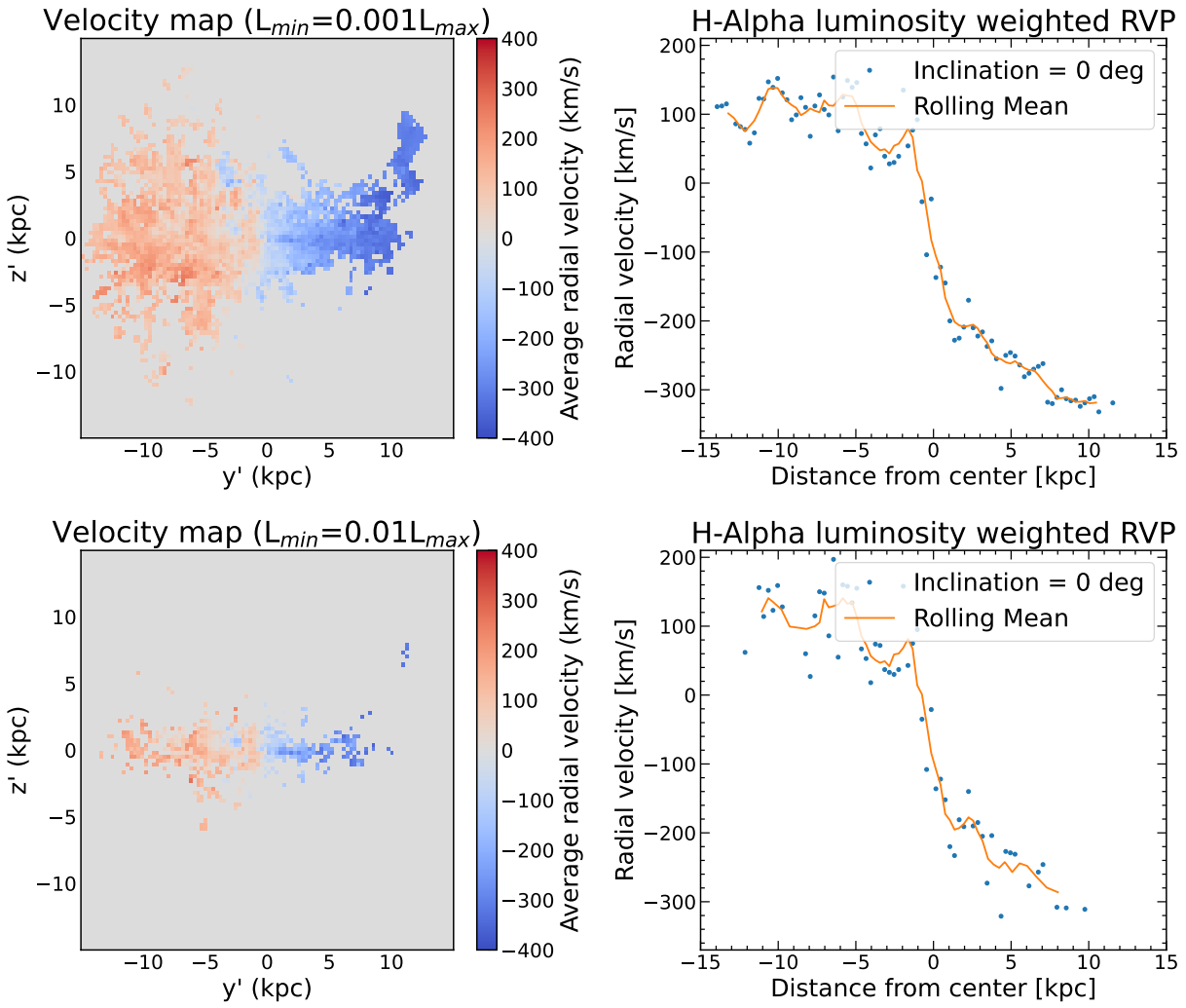

Figure 4.6: RVP for a 0° inclination (edge-on). The top row shows the RVP for a 0.1% limitation while the bottom row shows the RVP for a 1% limitation. What differentiates the two RVPs is the amount of data points used in the RVP. While both RVPs have a similar shape, the 0.1% limitation RVP has a clearer trend.

The rotational velocity that was calculated using Eq. 3.19 was averaged at every radius. The RVCs were turned into RVPs, which were then plotted alongside the inclination-corrected RVPs in Fig. 4.8. Fig. 4.10 shows the result of this.

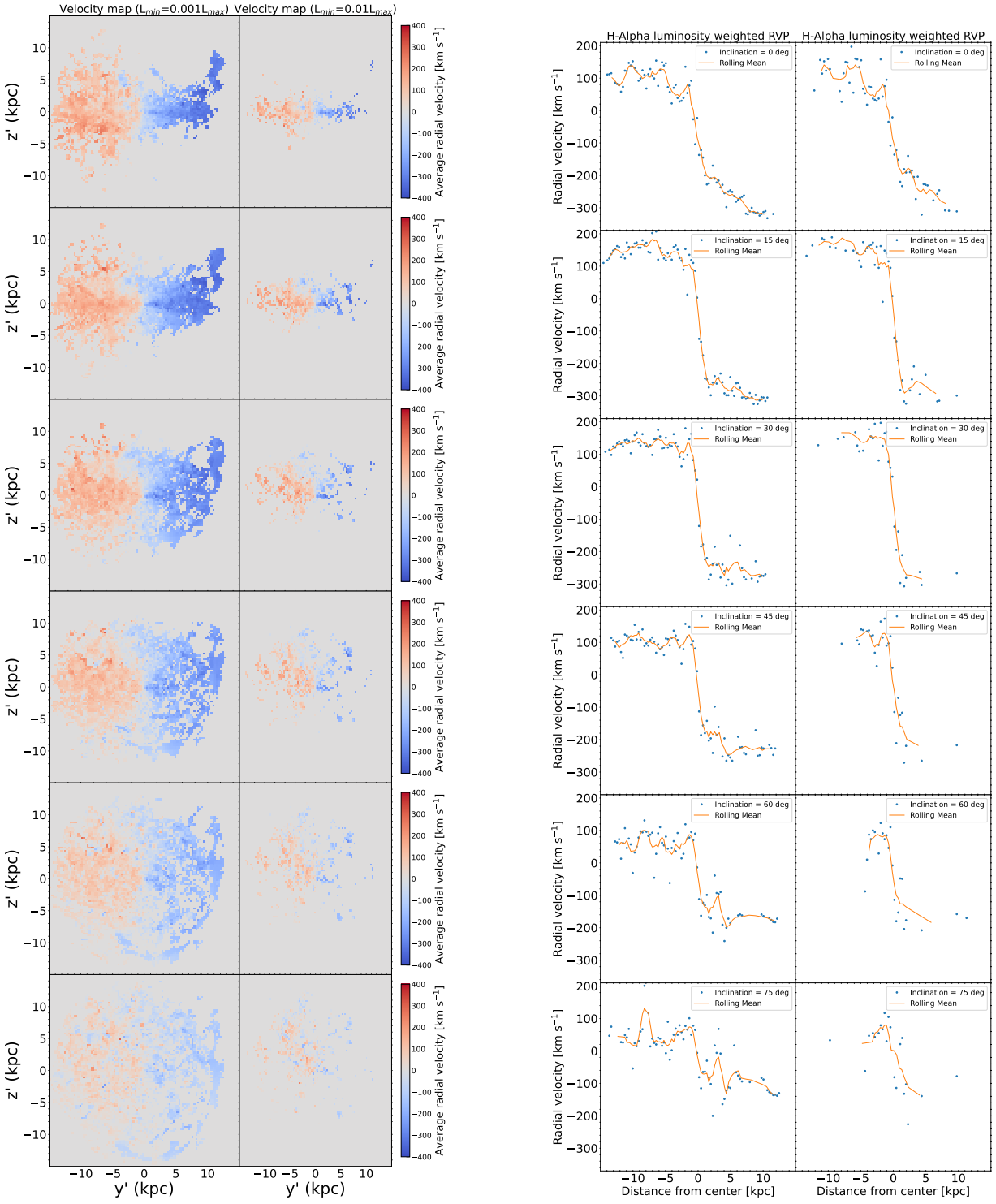

Figure 4.7: The two columns to the left display the two different luminosity-limited velocity maps, and their corresponding RVPs to the right. A rolling mean with window size 3 has been plotted with the RVP data to show the trends. The two velocity map columns are for 0.1% limitation and 1% limitation respectively. From top to bottom, this was done for 0°, 15°, 30°, 45°, 60°, and 75° inclinations.

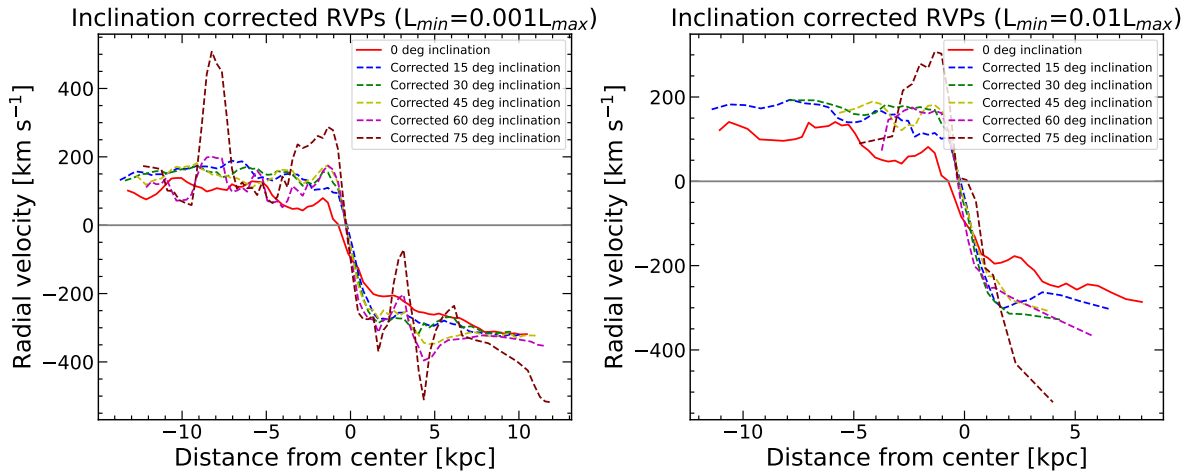

Figure 4.8: (Left) The inclination corrected RVPs for the angles 0°, 15°, 30°, 45°, 60°, 75° with a 0.1% limitation. (Right) The inclination corrected RVP for the angles 0°, 15°, 30°, 45°, 60° and 75° with a 1% limitation. The red line in both images shows the 0° inclination RVP while all the dotted lines show the inclination corrected RVPs at their respective luminosity limitations and inclination angles. A gray line has been drawn at zero radial velocity in order to clearly see the differences between positive and negative radial velocities.

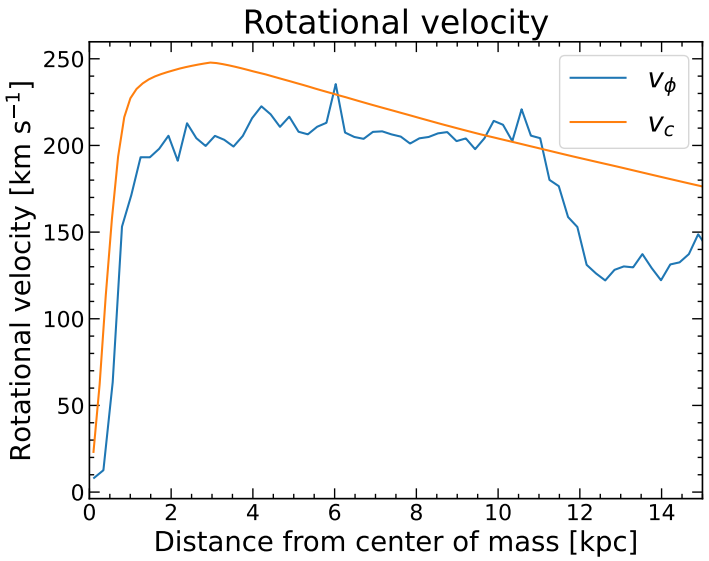

Figure 4.9: The two versions of theoretical RVCs plotted alongside each other. The yellow graph plots the rotational velocity v_c by applying Newtonian mechanics assuming a completely circular orbit using Eq.(3.21). The blue graph plots the rotational velocity v_ϕ using Eq.(3.19) which utilizes the position and velocity vector of the cells, and was then spatially averaged at every radii.

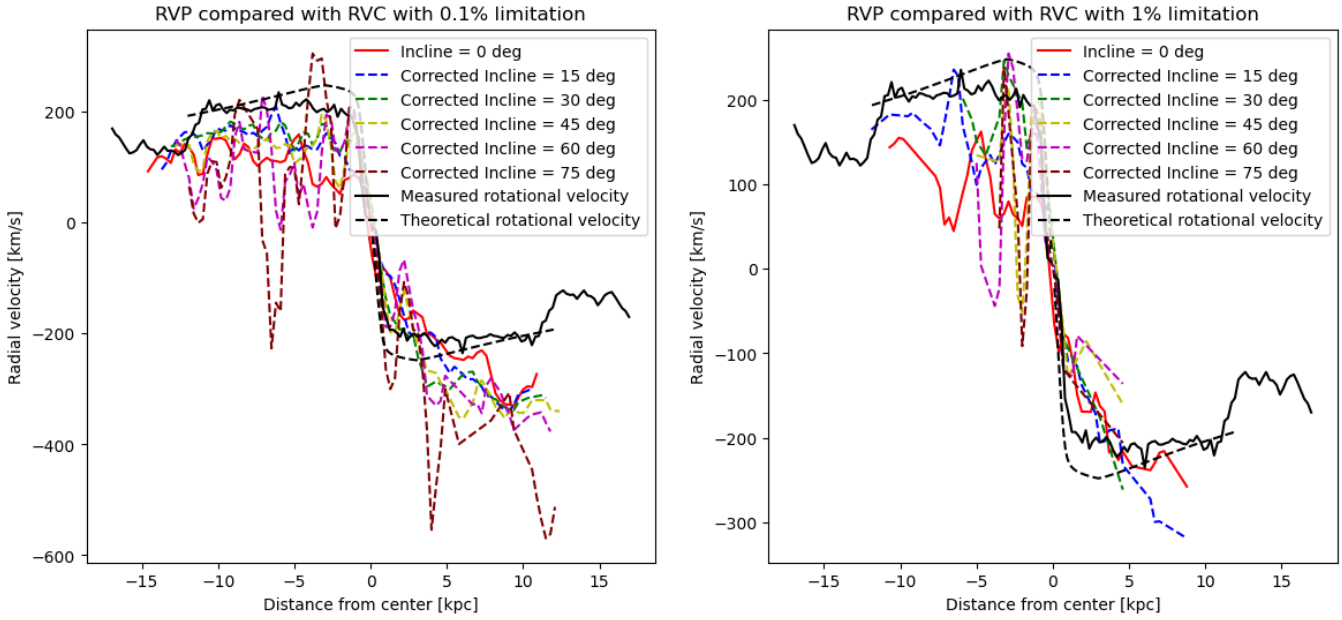

Figure 4.10: The black graphs the two theoretical RVCs reflecting both left and right side of the center of the galaxy by converting the rotational velocity to edge-on radial velocity. They are being compared to the colored graphs, which are the previously derived RVPs, to identify similarities and differences. The black graphs are symmetrical about $v_{rad} = 0$ by design, but the RVPs are not symmetrical about $v_{rad} = 0$, and instead appear shifted downwards.

Chapter 5

Discussion

This study investigated whether $H\alpha$ is a good gas tracer for the purpose of recovering the edge-on RVP of a galaxy from different observed inclinations. The resulting plots in Fig.4.10 suggest that it is not. Since the edge-on RVPs cannot accurately be turned into an RVC due to the asymmetries, the Hα-emission alone cannot recover the dynamical mass of the galaxy.

The analysis carried out in this thesis was done by calculating the angular momentum of a simulated galaxy, and using it to create a new coordinate system where the galaxy is observed edge-on, and then was inclined at 15°, 30°, 45°, 60° and 75°. The image at all times was 100x100 pixels large and covered an area of 30kpc×30kpc. At each inclination, the radial velocity was determined by taking the luminosity-weighted average velocity of a 1D-radial velocity histogram with bin size Δv = 2km/s along each column in the line of sight, which reflects the velocity one would measure from the $[H\alpha]\lambda$6564.6 Å line. The monochromatic luminosity was limited to 1% and 0.1% of the maximum monochromatic luminosity to reflect the data loss due to the distance to the galaxy and any possible disturbances along the path. The RVP for each inclined image at different limitations was then produced by taking the radial velocity for each pixel along $z' = 0$, the major kinematic axis. Two theoretical RVCs were then produced and compared to the measured RVPs. If v_ϕ would have been recovered from the RVPs and then used to calculate v_c, the dynamical mass of the galaxy could have been estimated.

Calculating the position of the center of mass and using the angular momentum vector to define a new coordinate system worked very well based on Fig. 4.4. Reducing the data using a percentage of the maximum monochromatic luminosity did work, but not optimally. The histogram containing the largest monochromatic luminosity in Fig. 4.5 shows a peak not grouped with the rest. Using this as the maximum luminosity removed more data than necessary. It would have been better to start with a minimum detectable flux and work out the minimum detectable luminosity if the distance to the galaxy had been known. Even though less data was used than desired, correcting for the different inclinations worked out fine based on Fig. 4.8. However, they were not possible to turn

into RVCs due to asymmetries made clear by the gray line separating positive and negative velocities and is made more clear in Fig. 4.10. The two theoretical RVCs do not match either and were not able to be correlated.

A reason for the asymmetries in the RVPs can be explained by the velocity maps at large inclinations in Fig. 4.7. There it becomes clear that gas with negative velocities overlaps to the half of the galaxy with positive velocities. The alternate method used a weighted average of a 1D-radial velocity histogram. Naturally, this means that if more gas with negative velocities is present, the weighted average velocity will become more negative. The reason for this gas with negative velocities being observed could be due to the fact that Hα can be emitted by very diffuse gas and thus very prone to turbulence. This causes outflows that do not give measurements that accurately describe the kinematics of the galaxy. A way to possibly work around this is to investigate another emission line possibly less affected by turbulent gas, such as the $[O_{II}]\lambda\lambda 3726, 3729$ Å doublet. The reason it was not included in this project is that no analytical solution was found that can describe the O_{II} luminosity. One could try to simulate an emission line and perform measurements on that. However, as mentioned in (Olsen et al. 2018), this is a challenge and was not successfully done in this study. If the RVP is then successfully recovered and used to determine v_ϕ, one can use asymmetric drift corrections to account for turbulent gas and get v_c by the equation

$$v_c^2 = v_\phi^2 - \frac{R}{\rho}\frac{dP}{d\rho}\ , \tag{5.1}$$

where R is the radius of the galaxy, ρ is the gas density and P is the pressure (Rey et al. 2024).

Velocity resolution and distance to the galaxy both play key roles in determining how much information we can gather from the light that can be observed. In this project, a velocity resolution of $\Delta v = 2$km/s was used (R=150'000), and an image size of 100×100 pixel grid which corresponds to a 30kpc × 30 kpc image. This is meant as an optimistic view in order to get clear enough data to perform the analysis. For telescopes such as KMOS, these values are different. KMOS has a spectral resolution of R=3700 ($\Delta v = 81.1$ km/s) and a spatial sampling of 0.2"x0.2" (Sharples 2011). With that size, the distance to the galaxy in this project (30kpc×30kpc covering 100x100 pixels) would be 309.4Mpc. Using Hubble's law and Eq. 2.2, this would mean a redshift of $z \approx 0.072$. By using the rest wavelength of Hα (6564.6 Å) and the ranges of KMOS (8'000Å - 25'000Å) in Eq.(2.2), the range of the redshift z is 0.22-2.8 for KMOS, meaning the assumptions used is not enough to observe Hα emission from this galaxy. Had the distance been known before alongside the diameter of the galaxy, the calculations can be reversed to determine the amount of pixels the image should cover. So a galaxy of 30kpc diameter with a distance of z=0.7 away from us would mean the pixel grid covering the galaxy is 10×10 pixels, as measured by KMOS. At larger redshift or smaller diameter, the pixel grid would have been even smaller. Using this pixel grid for this project would not yield any conclusion about the analysis as not enough data would be produced. That is why the assumption of 100x100 pixels is instead

assumed possible for future telescopes. With a known distance and a minimum detectable flux, the minimum detectable luminosity can be calculated using the luminosity distance formula. The data set can then be correctly reduced, accounting for the distance. The fluxes from the "surviving" luminosities can then be calculated to reflect the measurements KMOS would gather. If the RVC is computed from the simulation using these fluxes, it can be compared to one done by the $^{3D}BAROLO$ code that creates an RVC from a real data set (Di Teodoro & Fraternali 2015).

For future work, one may create more precise measurements, such as measured flux and image resolution, by including the actual distance to the galaxy, the specs of the observing telescope, investigating other possible emitters in the analysis, and derive more data such as gas density and pressure in order to use Eq. 5.1 if v_ϕ is successfully recovered. This would then give a more conclusive result as one can work backward with Newtonian mechanics to get the dynamical mass of the galaxy based on the derived v_c. This can then be compared with the known dynamical mass from the simulation in order to see if this method of recreating the RVC works and can be used to validate future simulations that try to replicate observed galaxies.

Bibliography

Abadi, M. G., Navarro, J. F., Steinmetz, M., & Eke, V. R. 2003, ApJ, 597, 21

Agertz, O., Renaud, F., Feltzing, S., et al. 2021, MNRAS, 503, 5826

Alpher, R. A., Bethe, H., & Gamow, G. 1948, Physical Review, 73, 803

Ashraf, M., Jose, J., Herczeg, G., & Fang, M. 2023, Journal of Astrophysics and Astronomy, 44, 67

Binney, J. & Tremaine, S. 1987, Galactic dynamics

Brinchmann, J., Charlot, S., White, S. D. M., et al. 2004, MNRAS, 351, 1151

Di Teodoro, E. M. & Fraternali, F. 2015, MNRAS, 451, 3021

Ejdetjärn, T., Agertz, O., Östlin, G., Renaud, F., & Romeo, A. B. 2022, MNRAS, 514, 480

Geach, J. E., Smail, I., Best, P. N., et al. 2008, MNRAS, 388, 1473

Governato, F., Willman, B., Mayer, L., et al. 2007, MNRAS, 374, 1479

Hahn, O. & Abel, T. 2011, MNRAS, 415, 2101

Hubble, E. P. 1936, Realm of the Nebulae

Mo, H. J., Mao, S., & White, S. D. M. 1998, MNRAS, 295, 319

Naidu, R. P., Conroy, C., Bonaca, A., et al. 2021, ApJ, 923, 92

Olsen, K., Pallottini, A., Wofford, A., et al. 2018, Galaxies, 6, 100

Perlmutter, S., Aldering, G., Goldhaber, G., et al. 1999, ApJ, 517, 565

Press, W. H. & Schechter, P. 1974, ApJ, 187, 425

Rey, M. P., Orkney, M. D. A., Read, J. I., et al. 2024, MNRAS, 529, 2379

Schmidt, M. 1959, ApJ, 129, 243

Schneider, P. 2006, Extragalactic Astronomy and Cosmology: An Introduction, 2nd edn. (Berlin, Germany: Springer)

Sharples, R. 2011, in Galaxy Formation, P160

Sharples, R. M., Bender, R., Hofmann, R., Genzel, R., & Ivison, R. J. 2003, in Society of Photo-Optical Instrumentation Engineers (SPIE) Conference Series, Vol. 4841, Instrument Design and Performance for Optical/Infrared Ground-based Telescopes, ed. M. Iye & A. F. M. Moorwood, 1562–1571

Swinbank, A. M., Harrison, C. M., Trayford, J., et al. 2017, MNRAS, 467, 3140

Tinsley, B. M. 1980, , 5, 287

Turk, M. J., Smith, B. D., Oishi, J. S., et al. 2011, , 192, 9

Zwicky, F. 1933, Helvetica Physica Acta, 6, 110